A Study of Highly Accurate Calibration based on Multiple 6-axis IMUs

Yutaka Shinkai[1,a)] Yoshiki Yamaguchi[2,b)]

Abstract: Uncrewed vehicles enable to support various situations, which exhibits tremendous power in a future aging society. Recent evolution in Global Positioning System (GPS) and Micro Electro Mechanical Systems (MEMS) technology accelerates this trend. For example, it makes information systems ultra-compact and ultra-lightweight, making high-frequency, high-precision data measurement more accessible. Thus, the current car navigation obtains the accurate attitude angle and trajectory of a running vehicle on a two-dimensional plane using multiple inertial sensors and a global positioning system. However, it sometimes faces unstable control based on inaccurate information not to work GPS appropriately, such as multipath error and location inside buildings, tunnels, and basements. To improve the accuracy, this article marshals the initial calibration approach of a triaxial accelerometer, and it focuses on the adjustment approach by numerical calculation without any specialized calibration equipment. Then, the selected calibration records the trajectory of a running vehicle. Consequently, this article discusses the characteristics of the approaches and concludes the better process from the viewpoint of actual use by comparing the experimental results.

Keywords: Multiple IMUs, Calibration, Inertial Navigation

1. Introduction

The recent development and evolution of Micro Electro Mechanical Systems (MEMS) technology has brought us ultra-small and ultra-lightweight sensors for information systems, making high-frequency and high-precision data measurement more accessible. A variety of fields, including automobiles, industrial devices, mechanical systems, mobile devices, and drones, adopt the MEMS-based accelerometers [1, 2]. In addition, systems that combine multiple sensors, such as a MEMS sensor (accelerometer + gyroscope) and Global Positioning System (GPS), are now widely adopted for the advanced position and velocity estimation of systems in which sensors are embedded. On the other hand, the rapid increase in the number of applications that accurate measurements for a long time require technological innovation in error correction methods for self-positioning.

The problem with exiting self-positioning systems is that their availability is limited to the space where GPS functions. For example, it is difficult to apply the system to self-driving drones and self-driving robots for surveillance and rescue in high-rise buildings over 1,000 meters high, attracting attention in the 21st century. Although it can install and operate many position sensors such as beacons inside buildings, basements, and tunnels, installation costs and maintenance are undesirable. In other words, it is desirable to be able to guarantee a sure positional accuracy for a certain period using only MEMS sensors. Thus, this article first focused on the discussion of initial calibration [3–5]. Significantly, this article focused on calibrating the obtained data only by information processing, without using any calibration device. Then, the initial calibration of the 3-axis accelerometer approaches is introduced, and the gains and losses to static measurements are discussed. After that, the pros and cons are described when applying the calibration method to dynamic measurements taken with a 6-axis sensor installed in a vehicle that performs position estimation.

The remainder of this article is structured as follows. The following section summarizes the error sources of the accelerometer. Sections 3 and 4 show the calibration method of the accelerometer and the results of preliminary experiments using actual machines, respectively. Section 5 shows the computational process for self-positioning, and section 6 offers the possibility of improvements in the self-positioning of vehicles. Section 7 closes with a conclusion and outlook.

2. Error Factors in Acceleration Sensors

Assuming that the true value of acceleration is T, the measured value by an IMU is M, and the error between the true value and the measured value is E, equation (1) can be obtained as the following.

$$E = M - T \tag{1}$$

Since the error E depends on the true value T, approximating it as a linear equation yields equation (2).

$$E = e_0 + e_1 \times T \tag{2}$$

From equations (1) and (2), equation (3) is derived.

$$M = e_0 + (1 + e_1) \times T \tag{3}$$

[1] Graduate School of Science and Technology, University of Tsukuba, 1-1-1 Tennodai, Tsukuba, Ibaraki 305-8577 Japan
[2] Faculty of Engineering, Information and Systems, University of Tsukuba, 1-1-1 Tennodai, Tsukuba, Ibaraki 305-8573 Japan
[a)] shinkai@hpcs.cs.tsukuba.ac.jp
[b)] yoshiki@cs.tsukuba.ac.jp

In equation (3), when $T = 0$, $E = e_0$. This e_0 is called the $0G$ error. The e_1 corresponds to the deviation of the sensor sensitivity and is called the sensitivity error. Thus, there are three principal categories of errors: $0G$ error, sensitivity error, and error by random noise. This article does not treat random noise.

Secondly, the acceleration T includes the gravitational acceleration (**G**), which is $1G = 9.80665\ [m/s^2]$, on the face of the globe. Assuming no errors, the relationship between the vector of measurements (ax, ay, az) and the **G** can be shown as equation (4).

$$ax^2 + ay^2 + az^2 = (1G)^2 \tag{4}$$

3. Acceleration sensor calibration methods and preliminary experiments

This article discusses how to improve the accuracy by referring to the previous proposed approaches. This section introduces these three calibration approaches [3–5] and the accuracy improvement for static acceleration.

3.1 Calibration by the least-squares method using six points with known acceleration at rest in each axis [3]

The initial calibration transform matrix can be obtained by the comparison of the **G** $(=1G)$ without errors and raw measurements at the stationary condition. The relationship between the accelerometer raw measured measurements (a_x, a_y, a_z) and the normalized values (A_x, A_y, A_z) can be expressed as the following equation.

$$\begin{bmatrix} A_x & A_y & A_z \end{bmatrix} = \begin{bmatrix} a_x & a_y & a_z & 1 \end{bmatrix} \begin{bmatrix} ACC_{11} & ACC_{21} & ACC_{31} \\ ACC_{12} & ACC_{22} & ACC_{32} \\ ACC_{13} & ACC_{23} & ACC_{33} \\ ACC_{10} & ACC_{20} & ACC_{30} \end{bmatrix} \tag{5}$$

Here, simplifying equation (5), equation (6) can be obtained.

$$Y = w \cdot X \tag{6}$$

The calibration parameter matrix X can be determined by the least-squares method, shown as equation (7).

$$X = (w^T \cdot w)^{-1} \cdot w^T \cdot Y, \tag{7}$$

where w^T and $(w^T \cdot w)^{-1}$ means a transposed matrix and an inverse matrix, respectively.

3.2 Error Estimation Method Using Ellipsoid Model [4]

Assuming an ideal state with no $0G$ error and no sensitivity error, the output of the accelerometer appears on a sphere of radius 1, as shown in equation (4). If the scales due to sensitivity error and translation due to $0G$ error are taken into account for each of the x, y, and z axes, equation (4) becomes an axis-aligned ellipsoid as shown in equation (8) instead of a sphere.

$$\left(\frac{x-p}{a}\right)^2 + \left(\frac{y-q}{b}\right)^2 + \left(\frac{z-r}{c}\right)^2 = (1G)^2 \tag{8}$$

There are six unknowns in equation (8), which can be evaluated by solving simultaneous equations with 6 different measurements. To improve the calibration correction, it is expected the 6 different measurements should be selected from the location which stays far apart from one another on the three-dimensional space.

3.3 Error estimation for each axis [5]

Assuming that the three orthogonal axes on the accelerometer are x_s, y_s, and z_s, and the vertical direction in the earth-centered coordinate system is the z-axis as shown in Figure 1.

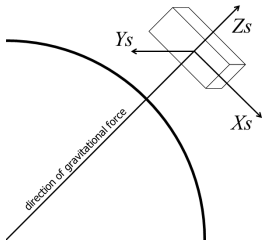

Fig. 1 $X_sY_sZ_s$ coordinate system for an IMU

According to each direction, six measurements are taken in the positive and negative directions. For example, considering the values of both positive and negative positions of the x_s direction, equations (9) and (10) can be derived from equations (3).

$$M_{x_{s+}} = e_0 + (1 + e_1) \times T \tag{9}$$

$$M_{x_{s-}} = e_0 - (1 + e_1) \times T \tag{10}$$

By rearranging these equations (9) and (10), e_0 can be obtained from equation (11).

$$e_0 = \frac{M_{x_{s+}} + M_{x_{s-}}}{2} \tag{11}$$

Then, e_1 is obtained by substituting e_0 from equation (11) and $T = 1G$ (at rest) into equations (9) and (10).

4. Acceleration sensor calibration methods and preliminary experiments

4.1 Preliminary experimental environment

For the preliminary experiments, four Digilent Pmod NAVs (ST LSM9DS1) were connected to a Digilent ANVYL FPGA board. Figure 2 shows the experimental apparatus used in the experiment, and Table 1 overviews the configuration of the Pmod NAV.

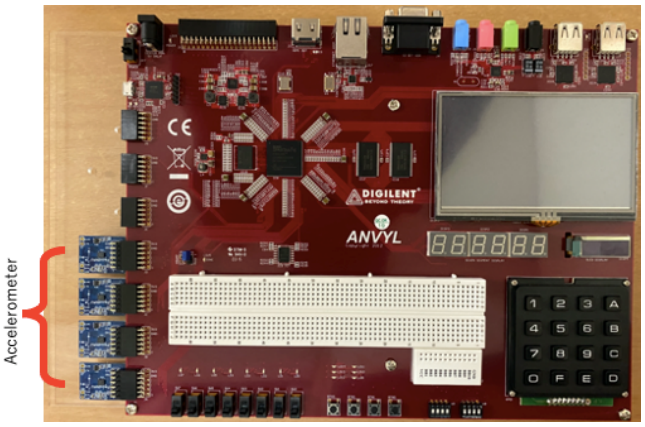

Fig. 2 Pmod NAV and FPGA board used in experiment

Table 1 Configuration of Pmod NAV with ST LSM9DS1

Accelerometers Range	±2 [g]
Gyroscope Range	±245 [degree/s]
Packet Output Rate	100 [Hz]

4.2 Preliminary experimental conditions

Real-time and field IoT systems need to mention the sensing issues affected by physical and digital butterfly effects [6]. A preparatory experiment was undertaken to get a better grasp of the characteristics of Pmod NAV; whose purpose is the evaluation of variability in them.

We measured the stopping data of six points at rest with respect to a flat table and a wall perpendicular to the table so that each axis had a known static acceleration. The measurement system was fixed in each direction, and the stopping data were measured five times at each point for 30 seconds so that each axis was in the direction of gravity and reverse direction of gravity, and the average value was used to obtain the calibration parameters.

4.3 Variability in sensor data

The accelerometer was placed on a flat floor at an interval of 2 meters from the floor to the east and west, and the data was collected at three different locations. Figure 3 shows a scatter plot of the output values on the x and y axes.

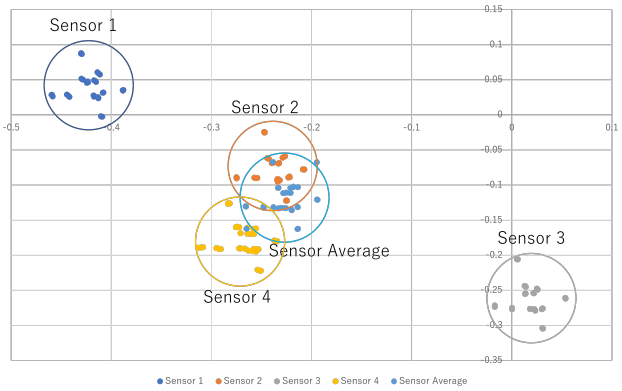

Fig. 3 Output value of each sensor and its average when stopped

Figure 3 illustrates two types of variability: the data variation depending on the sensing location and the character of each sensor. The former has less influence and is negligible. Thus, the averaging procedure was adopted using multiple sensors to reduce the impact of the latter.

4.4 Reference data without calibration

First of all, the reference data of a stationary state were prepared for the comparison of calibration approaches. The reference data was obtained by multiple 6-axis sensors embedded on a proposed system configuration, which are shown in Figure 2. The system was located on a flat floor whose z-axis was set in the direction of gravity. It was rotated 0°, 90°, 180°, and 270° degrees in the x-y plane normal to the gravity axis, and measured the state in each location. The data was measured five times at each point, and the average values were used as the representative value. The calibration method shown in Sections 3.1 ∼ 3.3 is applied to these representative values, and the difference are discussed in this section. The accuracy was adopted as the index of this discussion, and the comparison was based on the obtained composite vectors of 3-axis acceleration to the gravitational acceleration of 9.800 $[m/s^2]$ in [7].

Although there was some variation among the sensors, there was no significant difference in the trend of the acquired data if each sensor, so only the results of two sensors are shown. Table 2 shows the acceleration data at rest before calibration.

Table 2 Accelerometer output before calibration

	Accelerometer 1			Accelerometer 2		
Rotation	ax1	ay1	az1	ax2	ay2	az2
0	-0.361	-0.023	9.758	0.036	-0.194	9.754
90	-0.374	-0.044	9.757	0.022	-0.215	9.756
180	-0.390	-0.047	9.758	0.003	-0.217	9.758
270	-0.395	-0.008	9.759	0.005	-0.178	9.756
	9.765 $[m/s^2]$			9.758 $[m/s^2]$		

4.5 Experimental results with calibrations

4.5.1 Calibration by Least Squares Method (Section 3.1)

Table 3 shows the calibration results. The composite vectors are closer to the gravity acceleration of 9.800 $[m/s^2]$ in Ibaraki Prefecture compared to Table 2 before calibration. In addition, the output of x and y axes converged to around zero. From this, we can assume that the method in Section 3.1 is performed so that the sensor is perfectly perpendicular to the ground.

Table 3 Calibration by Least Squares Method (Section 3.1)

	Accelerometer 1			Accelerometer 2		
Rotation	ax1	ay1	az1	ax2	ay2	az2
0	0.023	-0.008	9.789	0.019	-0.009	9.796
90	0.010	-0.029	9.788	0.005	-0.030	9.797
180	-0.006	-0.032	9.790	-0.015	-0.037	9.799
270	-0.011	0.008	9.790	-0.012	0.007	9.797
	9.790 $[m/s^2]$(9.765 $[m/s^2]$)			9.797 $[m/s^2]$(9.758 $[m/s^2]$)		

4.5.2 Calibration with the ellipsoid model (Section 3.2)

Table 4 shows the calibration results. The composite vectors are closer to the target values, and the difference is that the output of the x and y axes remain when compared to Table 3. In the method of Section 3.2, it is thought that the sensor is calibrated to align the z-axis with the direction of gravity, taking into account the tilt of the sensor.

Table 4 Calibration with Least Squares Method (Section 3.2)

	Accelerometer 1			Accelerometer 2		
Rotation	ax1	ay1	az1	ax2	ay2	az2
0	-0.081	-0.004	9.798	0.094	-0.012	9.795
90	-0.095	-0.024	9.797	0.080	-0.033	9.797
180	-0.110	-0.027	9.798	0.061	-0.035	9.799
270	-0.116	0.012	9.799	0.063	0.004	9.797
	9.798 $[m/s^2]$(9.765 $[m/s^2]$)			9.797 $[m/s^2]$(9.758 $[m/s^2]$)		

4.5.3 Calibration results by error estimation for each axis (Section 3.3)

Table 5 shows the calibration results. The output values of each axis as well as the composite vector were the same as in Table 4.

Table 5 Calibration using the error average method (Section 3.3)

	Accelerometer 1			Accelerometer 2		
Rotation	ax1	ay1	az1	ax2	ay2	az2
0	-0.081	-0.004	9.798	0.094	-0.012	9.795
90	-0.095	-0.025	9.797	0.080	-0.033	9.797
180	-0.110	-0.028	9.799	0.061	-0.035	9.799
270	-0.116	0.011	9.799	0.064	0.004	9.797
	9.799 $[m/s^2]$(9.765 $[m/s^2]$)			9.797 $[m/s^2]$(9.758 $[m/s^2]$)		

4.6 Summary of preliminary experiments

Table 3, Table 4 and Table 5 show that the composite vector after calibration approaches the target values of 9.800 $[m/s^2]$ for all calibration methods. In particular, the methods in Sections 3.2 and 3.3 yielded similar results for the values of each axis. The method in Section 3.3 requires that the data be measured with each axis pointing exactly in the direction of gravity and in the reverse direction of gravity. In the method of Section 3.2, the stopping data for calibration is in an arbitrary direction. For the flexibility of the calibration method, the calibration method in Section 3.2 is used in the vehicle driving experiments.

Next, we focused on the values of the x and y axes after applying the calibration methods of the Section 3.1 and 3.2. There was a large difference in the results between the two calibrated values. However, it is difficult to say which of the calibration methods in Section 3.1 and 3.2 is superior in this experiment at static acceleration. Therefore, we will compare the two calibration methods using Section 3.1 and 3.2 in a vehicle driving experiment.

5. Self-Positioning Method

Next, as a method to evaluate the inertial calibration of the accelerometer against dynamic acceleration, we used the self-position estimation method using a vehicle. Although GPS is widely used for self-positioning of vehicles, there are many places where GPS information cannot be used, such as a tunnels and suburbs. To solve this problem, inertial navigation using only acceleration and gyroscope is used to calculate the driving route of the vehicle so that it ca be completed within the system.

5.1 Angle Definition and Absolute Coordinate System

6-axis sensor are widely used for motion measurement. The rotation of each axis is defined as roll angle(φ) for x-axis, pitch angle(θ) for y-axis, and heading angle(ψ) for z-axis. The reference coordinate system was defined as a right-handed coordinate system with the z-axis direction being the direction of gravity, and counterclockwise was the positive direction for rotation around each axis.

5.2 Initial Posture Angle [8]

In this report, the initial posture angle of the 6-axis sensor was calculated using the output value of the acceleration sensor at rest. Since the accelerometer detects only the gravitational acceleration at rest, the relation between the accelerometer and the gravitational acceleration in the absolute coordinate system is shown in equation (12).

$$ {}^{i}A = {}^{o}R_i^T \cdot {}^{o}A \tag{12} $$

$$ {}^{i}A = \begin{bmatrix} {}^{i}A_x \\ {}^{i}A_y \\ {}^{i}A_z \end{bmatrix} \tag{13} $$

$$ {}^{o}A = \begin{bmatrix} 0 \\ 0 \\ g \end{bmatrix} \tag{14} $$

${}^{i}A$ is the accelerometer output, ${}^{o}A$ is the acceleration at the origin O of the absolute coordinate system, ${}^{o}R_i$ is the rotation matrix from the sensor coordinate system to the absolute coordinate system and g is the gravitational acceleration. Since the rotation of each axis is applied in the order of roll, pitch and heading, ${}^{o}R_i$ can be shown in equation (15).

$$ {}^{o}R_i = \begin{bmatrix} \cos\psi & -\sin\psi & 0 \\ \sin\psi & \cos\psi & 0 \\ 0 & 0 & 1 \end{bmatrix} \cdot \begin{bmatrix} \cos\theta & 0 & \sin\theta \\ 0 & 1 & 0 \\ -\sin\theta & 0 & \cos\theta \end{bmatrix} \cdot \begin{bmatrix} 1 & 0 & 0 \\ 0 & \cos\varphi & -\sin\varphi \\ 0 & \sin\varphi & \cos\varphi \end{bmatrix} \tag{15} $$

Furthermore, using equations (13) and (14), the initial posture angle of the 6-axis sensor can be calculated form the static acceleration as flows.

$$ \begin{bmatrix} {}^{i}A_x \\ {}^{i}A_y \\ {}^{i}A_z \end{bmatrix} = \begin{bmatrix} -\sin\theta\, g \\ \cos\theta\sin\varphi\, g \\ \cos\theta\cos\varphi\, g \end{bmatrix} \tag{16} $$

$$ \varphi_0 = \tan^{-1}\frac{{}^{i}A_y}{{}^{i}A_z} \tag{17} $$

$$ \theta_0 = \tan^{-1}\frac{-{}^{i}A_x}{\sqrt{{}^{i}A_y^2 + {}^{i}A_z^2}} \tag{18} $$

ϕ_0 and θ_0 are the roll and pitch angle calculated from the static acceleration. However, it is not possible to obtain the initial heading angle from the only 6-axis sensor.

5.3 Coordinate Conversion of Gyroscope and Accelerometer [8]

Since integrating the output values of the gyro and accelerometer as they are does not give correct results, it is necessary to transform them from the sensor coordinate system to absolute coordinate system. The outline of the coordinate transformation is shown in Figure 4.

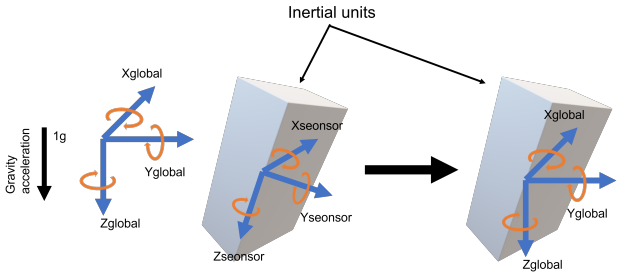

Fig. 4 Coordinate transformation from sensor coordinate system to absolute coordinate system

First, the coordinate transformation in the gyroscope is represented by equation (19), and the differential equation for roll, pitch and heading angles are shown.

$$\begin{bmatrix} \dot{\varphi} \\ \dot{\theta} \\ \dot{\psi} \end{bmatrix} = \begin{bmatrix} 1 & \sin\varphi\tan\theta & \cos\varphi\tan\theta \\ 0 & \cos\varphi & -\sin\varphi \\ 0 & \sin\varphi\sec\theta & \sec\theta \end{bmatrix} \begin{bmatrix} \omega_x \\ \omega_y \\ \omega_z \end{bmatrix} \quad (19)$$

ω_x, ω_y and ω_z are the output values of the gyroscope in the sensor coordinate system. The initial values of the roll and pitch angles are the ones calculated in equation (18). The coordinate transformation in the accelerometer can be done to the absolute coordinate system by applying equation (15) to the sensor acceleration. We used Eular angles as the rotation matrix because it can be assumed that gimbal lock does not occur during driving a vehicle.

6. Method and results of the vehicle experiment

In this Section, we show the results of vehicle routes obtained by applying calibration to dynamic acceleration.

6.1 Overview of the measurement system and experimental methods

Fourteen Pmod NAVs, one ADIS16497-2 (ANALOG DEVICES), two Spartan-6FPGA boards were used for data measurement. The settings of the various sensors are Table 1 for Pmod NAV and Table 6 for ADIS16497-2.

Table 6 Configuration of ADIS16497-2

Accelerometers Range	±40 [g]
Gyroscope Range	±450 ~ 480 [degree/s]
Packet Output Rate	100 [Hz]

The measurement system is installed at the foot of the passenger seat, and the scene is shown in Figures 5 and 6. This was because the measurement system was stable in the vehicle while driving, and the z-axis of the 6-axis sensor was facing the direction of gravity.

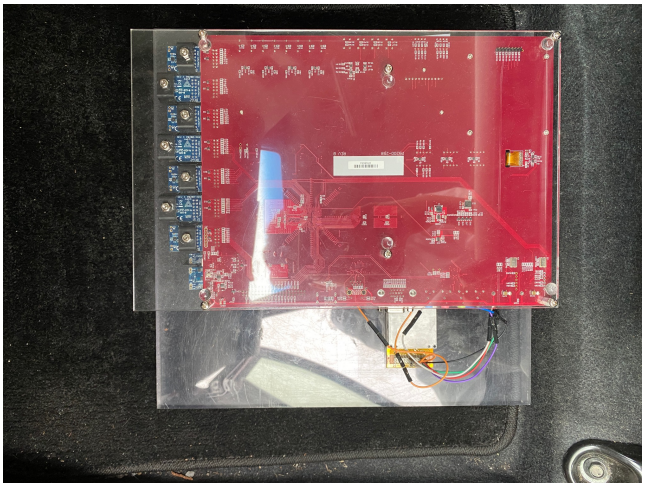

Fig. 5 Measurement system seen from above

The calibration parameters of the accelerometer were obtained off-line just before the vehicle experiment using the method described in Section 4.2. This is because it was difficult to estimate the calibration parameters while the vehicle was driving.

The purpose of this experiment was to investigate the effect of

Fig. 6 Measurement system seen from the side

initial calibration of accelerometer and averaging using multiple sensors on dynamic acceleration. Therefore, to see this effect, the calibration of the gyroscope was limited to applying only the removal of drift error. Specifically, the gyroscope was calibrated by stopping for 15 seconds before driving the route and subtracting the average value from all the gyroscope data to remove the drift error. In this experiment, the driving time was about 120 to 150 seconds including the stationary time, and the total driving distance was about 700 meters. For the sake of space, we show the route results for the four sensors, the route for the average of all 14 sensors, and the route for ADIS16497-2.

6.2 Route without initial acceleration calibration

First, a route based on the average of the fourteen Pmod NAV output values with drift error removal and without acceleration calibration is shown in Figure 7.

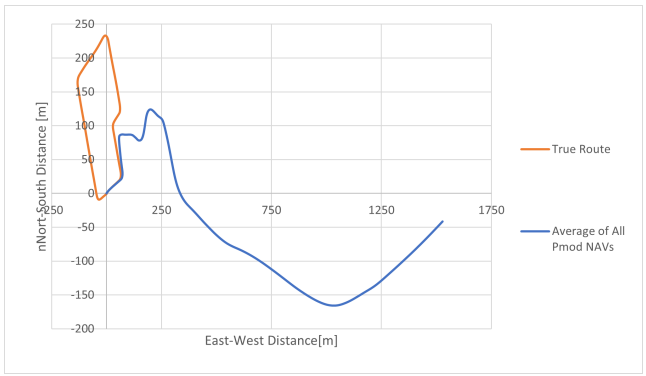

Fig. 7 Comparison of pre-calibration average and true value route

Without accelerometer calibration, the initial posture of the sensor could not be measured correctly due to both 0G error and sensitivity error in the accelerometer, and the error accumulated over time.

6.3 Trajectory with Calibration by Least-Squares Method (Section 3.1)

6.3.1 Route for each sensor

Compared to Figure 8, the distance traveled was closer to the actual route. In terms of the direction of driving, we were not able

to capture it correctly.

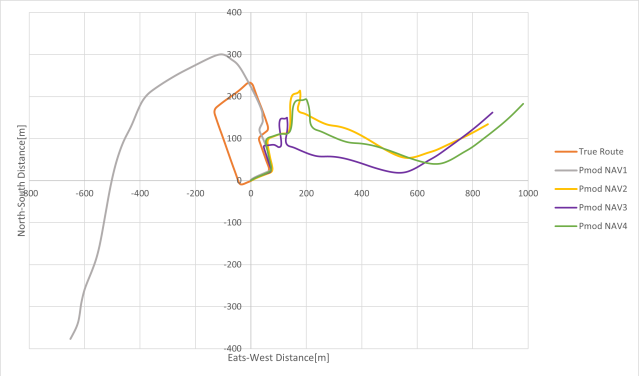

Fig. 8 Each Sensor Route with calibration (Section 3.1)

6.3.2 Average of all Pmod NAVs and ADIS16497-2

From Figure 9, whether 14 sensors or ADIS16497-2 are used, correct measurements were made in the first 20 seconds of driving, but errors accumulated as time passed, probably because the initial posture was not correct. We conducted several experiments, and the results in Figure 9 were similar in all cases.

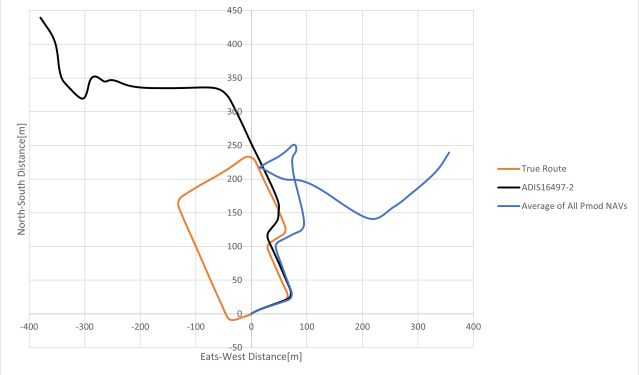

Fig. 9 Comparison of Average of All Pmod NAVs and ADIS16497-2 with calibration (Section 3.1)

6.4 Trajectory with Calibration by Ellipsoid Model (Section 3.2)

6.4.1 Route for each sensor

From Figure 10, the accuracy of the driving route for each sensor has been improved compared to Section 6.3.1. This can be attributed to the fact that the initial calibration of the accelerometer worked well, and the initial posture of the sensor was close to the correct value. Although it is getting closer to the true value route, the error is thought to increase over time due to noise during measurement because it is an expensive sensor.

6.4.2 All average and ADIS16497-2 (Master Data)

From Figure 11, by using the average value of 14 sensors, a significant improvement in accuracy was observed. We believe that this is because we were able to smooth out the noise that occurs during driving for each sensor. However, this is only the master data from several experiments. Figures 12, 13, and 14, described in the next section, are the result of several experiments (averaged of 14 Pmod NAVs with calibration applied by the ellipsoid model and comparing the routes with ADIS16497-2 with same calibration).

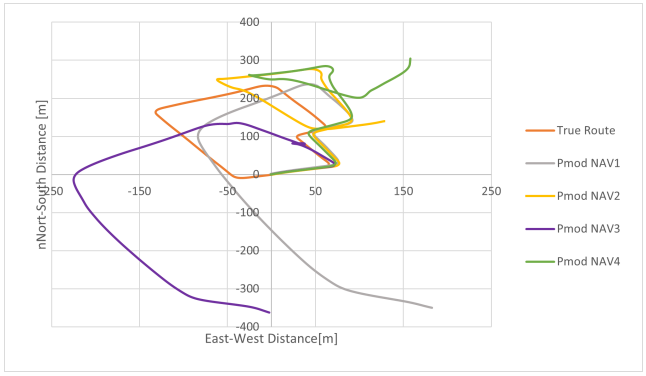

Fig. 10 Each Sensor Route with calibration (Section 3.2)

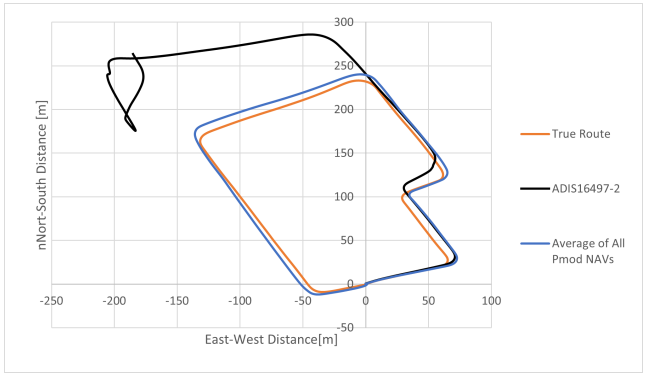

Fig. 11 Comparison of Average of All Pmod NAVs and ADIS16497-2 with calibration (Section 3.2)

6.4.3 All average and ADIS16497-2(Results of multiple experiments)

From these results, we can see that the expensive sensor (ADIS16497-2) has stability in the output value even when it is used alone. On the other hand, the inexpensive sensor (Pmod NAV) may have the same stability as ADIS16497-2 by using the average value of 14 sensors in this case.

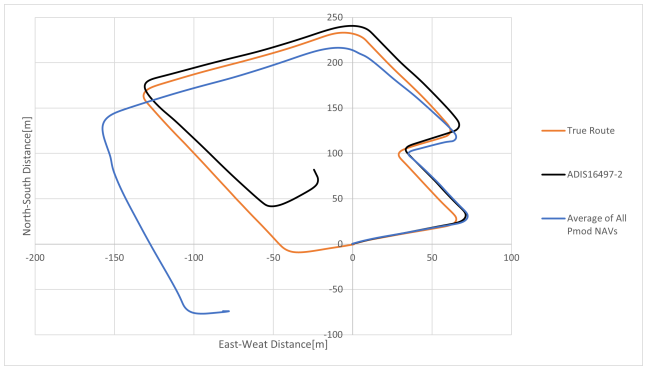

Fig. 12 Results of second experiment

7. Conclusions

This article discussed how large variety the accuracy of the trajectory log of a running vehicle is brought by the initial calibration method of the accelerometer. First, in Section 3.1, the calibration by the least-squares method was applied. However, the accuracy improvement was insufficient. In multiple trials, this approach detected the traveling direction of a target vehicle with sufficient accuracy. Still, the calculated distance and

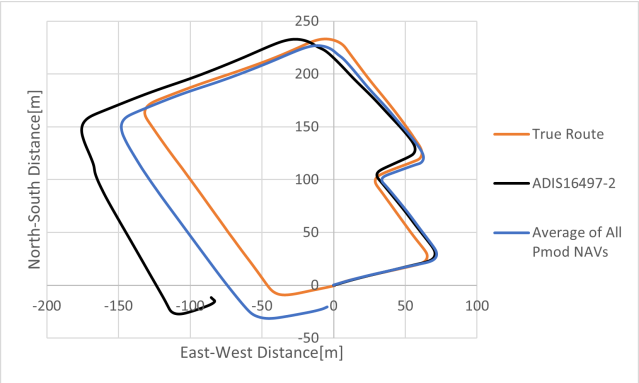

Fig. 13 Results of third experiment

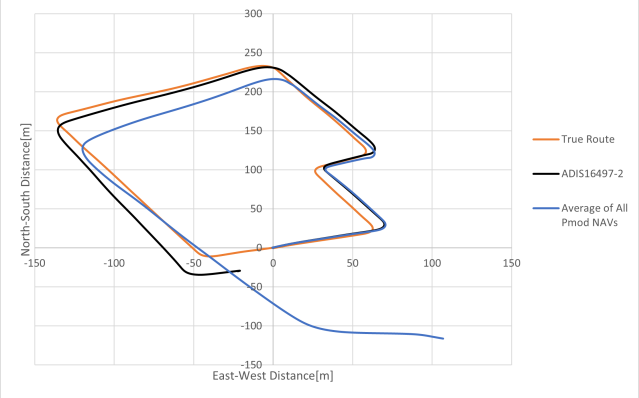

Fig. 14 Results of fourth experiment

direction traveled by the vehicle, etc., deviated significantly from the correct trajectory. The reason was why the initial posture calculated from the acceleration sensor at stationary state was incorrect.

Then, in Section 3.2, the calibration using the ellipsoid model was introduced. However, there was an improvement in accuracy for each Pmod NAV when introducing an averaged approach with multiple IMUs. The averaged value by multiple IMUs reduced the variety of each sensor. It implies that the larger the number of sensors is, the more accurate sensing the system will achieve.

Some wrong trajectories were obtained in the averaged approach when the roll and pitch angles were not well-detected. It influenced the gyroscope's roll and pitch angles, but the current approach can not reduce the effect. In future works, it is necessary to accurately correct accelerometers and gyroscopes during driving to enhance accuracy.

Acknowledgement

This work was supported in part by JSPS KAKENHI Grant Number JP19H00806, and TIA collaborative research program "KAKEHASHI" in FY2020 and FY2021. We also thank the Xilinx University Program for the kind donation of software tools.

References

[1] Tamagawa Seiki Co., Ltd.: *Technology of Gyroscope*, Tokyo Denki University Press (2011).
[2] Matsuhashi, H.: *Introduction to Semiconductor Sensors for Automotive Applications*, Kagakujoho shuppan Co., Ltd. (2016).
[3] STMicroelectronics: AN4508: Parameters and calibration of a low-g 3-axis accelerometer, DocID026444 Rev.1 (2014).
[4] Yamaguchi, K.: Error measurement of acceleration sensors, Computer Entertainment Supplier's Association (CESA) Developments Conference, pp.1–8 (2009).
[5] Hoshino, S.: A study of shape measurement by using acceleration, gyroscope, and rotational angle sensors, Master's thesis, Graduate School of Science and Technology, Gunma University (2019).
[6] Futagami, T. and Starrett, C.: Digital Butterfly as Research and Education Target, *Proceedings of Asia Pacific Conference on Robot IoT System Development and Platform*, pp. 1–2 (2018).
[7] Yahagi, T., Yoshida, K., Miyazaki, T., Hiraoka, Y. and Miyahara, B.: Establishment of the Japan Gravity Standardization Net 2016: JGSN2016, *Journal of the geodetic society of Japan*, Vol. 64, pp. 14–25 (2018).
[8] Hirose, K. and Kondo, A.: Special Issues No.3: Measurement Technique for Ergonomics, Section 1-2: "Measurement of Body Motion" –Motion Measurements by Inertial Sensors–, *Ergonomics*, Vol. 50, No. 4, pp. 182–190 (2014).